Available online at www.sciencedirect.com
SCIENCE DIRECT®
Acta Materialia 53 (2005) 1467–1478
Acta MATERIALIA
www.actamat-journals.com

Embrittlement of a bulk metallic glass due to sub-T_g annealing

P. Murali, U. Ramamurty *

Department of Metallurgy, Indian Institute of Science, C.V. Raman Avenue, Bangalore 560 012, India

Received 10 September 2004; received in revised form 24 November 2004; accepted 29 November 2004
Available online 5 January 2005

Abstract

The susceptibility of $Zr_{41.2}Ti_{13.75}Cu_{12.5}Ni_{10}Be_{22.5}$ (Vitreloy-1) bulk metallic glass (BMG) to embrittlement upon annealing at temperatures below its glass transition temperature, T_g, was investigated. Both isothermal annealing at 500 K ($0.8T_g$) for up to 24 h and isochronal annealing for 24 h in the temperature range of 400 K ($0.65T_g$) to 530 K ($0.85T_g$) were conducted and the impact toughness, Γ, values were measured. Results show severe embrittlement, with losses of up to 90% in Γ, with annealing. A one-to-one correspondence between Γ and the enthalpy change at the glass transition, ΔH, with annealing time, t_a, and temperature, T_a, was found, indicating that the reduction of free volume, v_f, due to annealing is the primary mechanism responsible for the loss in Γ. Since v_f also affects the viscoelastic response of the material, a dynamic mechanical analyzer has been used to study the changes in the internal friction, $\tan\delta$, and viscosity, η, due to annealing. The results show an increase of 30% in the η due to sub-T_g annealing. An instrumented indentation technique was utilized to examine the micromechanical reasons for the embrittlement. While the Vickers indentation response of the as-cast and annealed glasses do not show any significant difference, spherical indentation studies show a reduced shear band activity in the annealed BMG. Further, relatively high indentation strain was observed to be necessary for shear band initiation in the annealed glass, implying increased resistance for the nucleation of shear bands when the BMG is annealed.

Keywords: Bulk amorphous materials; Annealing; Differential scanning calorimetry; Embrittlement; Shear bands; Indentation

1. Introduction

Metallic glasses were initially produced using rapid quenching techniques by subjecting the molten alloys to very high cooling rates, $\sim 10^6$ K/s [1]. Since these metastable materials are trapped in local minima of free energy, they tend to change their structure progressively towards the crystalline state or more stable glassy states (ideal glass state) when they are supplied with the necessary thermal energy. This process is referred to as structural relaxation. Due to the rapid quenching, metallic glasses have considerable residual stresses within them, which are detrimental to their soft magnetic properties [2]. Low temperature (sub-T_g) annealing treatments are used in order to reduce the residual stresses, which would otherwise cause component distortion during service as well as affect functional properties. However, relaxation annealing was found to induce severe embrittlement, as measured by the loss of ductility in ribbon samples [3]. This is attributed to various factors, the most prominent being the reduction in free volume, v_f, which is defined as the portion of the volume surrounding an atom that can be exchanged with neighboring atoms without any expenditure of energy [3,4]. Flow mechanisms in metallic glasses are understood in terms of v_f, which can be thought of as "defects" in amorphous alloys similar to vacancies in crystalline materials [5–8]. During structural relaxation of metallic glasses excess free volume gets redistributed and annihilated, resulting in the loss of ductility [3].

* Corresponding author. Tel.: +91 80 2293 3241; fax: +91 80 2360 0472.
E-mail address: ramu@met.iisc.ernet.in (U. Ramamurty).

1359-6454/$30.00
doi:10.1016/j.actamat.2004.11.040

Several multi-component alloy systems that exhibit high glass forming ability were discovered recently [9,10]. Because of this ability, these alloys do not require very high rates of cooling to form amorphous solids and specimens in the bulk form can be produced. These are referred to as bulk metallic glasses (BMGs) and have unique combinations of mechanical properties that qualify them for consideration in structural applications where high performance is needed [11].

Because of the slower cooling during production, BMGs have densities similar to their crystalline counterparts [12]. This implies low quenched-in free volume vis-à-vis that in the rapidly quenched glasses. Despite this, preliminary investigations have shown that sub-T_g annealing imparts severe brittleness to the BMGs [12–14]. The reasons for this are not yet clear. Detailed understanding of the sources of the relaxation induced embrittlement is particularly important from the applications point of view, as embrittlement may result in restrictions in terms of the maximum allowable service temperatures for components made using the BMGs.

In this work, we examine the susceptibility to embrittlement of Vitreloy-1, which is an excellent glass former (critical cooling rate less than 10 K/s) and hence widely studied for its mechanical properties [9]. Specific objectives are to examine whether the variations of Γ with t_a and T_a can be correlated with changes in structural parameters that are readily measurable. We also seek to identify the alterations, if any, to the constitutive plastic flow that result in the embrittlement, through instrumented indentation experiments.

2. Material and experiments

Three mm thick as-received plate of the $Zr_{41.2}Ti_{13.8}Cu_{12.5}Ni_{10.0}Be_{22.5}$ (at.%) fully amorphous alloy with the commercial name of Vitreloy-1 was electro-discharge machined into notched bars (30 mm in length, 5 mm in width and 3 mm in thickness) with 2.5 mm deep notches. The machined samples were then vacuum-sealed and annealed at a temperature of 500 K ($0.8T_g$) for different time intervals, up to 24 h. The annealing time intervals, t_a, were chosen in such a way that the data points be spaced at roughly equal intervals when plotted in a logarithmic scale. Isochronal annealing experiments were conducted for 24 h at temperatures, T_a, in the range of 400–530 K that correspond to 0.65 and $0.85T_g$, respectively.

The as-cast and annealed alloys were characterized using X-ray diffraction (XRD) and differential scanning calorimetry (DSC). The XRD analysis was conducted using the Cu Kα radiation at a scan rate of 2°/min. Enthalpy changes after the annealing were calculated from thermograms obtained from the DSC data obtained using a heating rate, Φ, of 10 K/min in argon atmosphere.

The samples were polished to one μm finish by using a disk-polishing unit with diamond paste. Impact tests were carried out on the polished samples on an instrumented Charpy impact-testing machine with an impact velocity of 0.74 m/s. Complementary quasi-static 4-point bend tests on notched specimens (with 10 and 20 mm inner and outer spans, respectively) were performed in a universal testing machine at a displacement rate of 10^{-2} mm/s. Fracture morphologies were examined in a scanning electron microscope (SEM). The polished sides of the samples were examined in an optical microscope.

Viscosity was calculated from the measured internal friction from a dynamic mechanical analyzer (DMA) in a 3-point bend configuration (dimensions: 5×3 mm cross-section and 50 mm span) by applying an oscillatory load of 50 N and frequencies in the range 1–100 Hz.

Depth sensing indentations were conducted on the as-cast and annealed (T_a = 500 K, t_a = 24 h) samples using CSM micro hardness tester. Indentations were made using a spherical diamond indenter with radius R = 50 μm, by applying a maximum load, P_{max}, of 1, 5, 10 and 20 N. The loading and unloading rates were maintained at 2 N/min. Additionally, instrumented micro and nanoindentations were performed using a Vickers indenter. The micro-Vickers indentation experiments, with maximum load of 20 N and loading rates of 2 and 40 N/min, were conducted using the CSM microindenter. The nanoindentations were performed with a maximum load of 50 mN and loading and unloading rates of 0.1 mN/s, using a MTS nanoindenter.

3. Calorimetry

The XRD scans obtained for the as-cast and the annealed (t_a = 24 h, T_a = 500 K) samples are shown in Fig. 1. Since $T_a < T_g$, no perceptible crystallization is evident. A detailed structural characterization involves computing the partial pair correlation functions by combining data deduced from various scattering experiments (X-rays, neutron and electron diffraction etc.) in which each experiment gives its unique scattering function for a given pair of atoms [15]. Such a procedure has not been attempted on the multi-component BMGs as yet.

The DSC thermograms of the isothermal ($T_a = 0.8T_g$) and isochronal (t_a = 24 h) annealed samples are shown in Figs. 2 and 3, respectively. For the as-cast alloy, the T_g is 625 K whereas the first crystallization peak starts at a temperature, T_x, of 700 K. The wide super cooled liquid region ($T_x - T_g \sim 75$ K) for this alloy is an indicator of its excellent glass forming ability.

Similar to the XRD scans, a comparison between the DSC scans obtained from the as-cast and the annealed alloys shows no perceptible differences, except for the

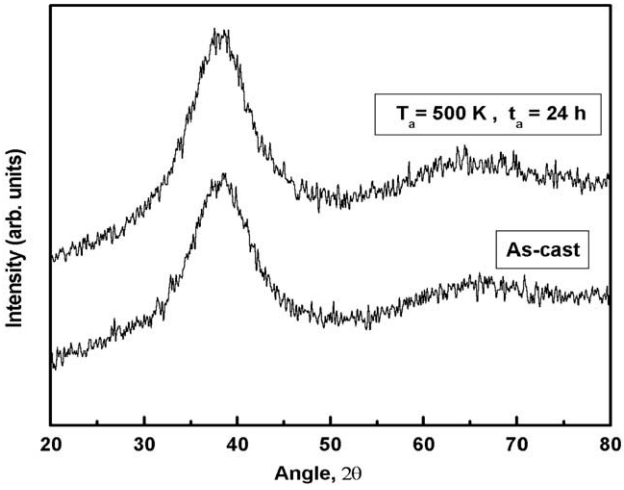

Fig. 1. X-ray diffraction patterns of the as-cast and 24 h annealed (at 500 K) $Zr_{41.2}Ti_{13.8}Cu_{12.5}Ni_{10.0}Be_{22.5}$.

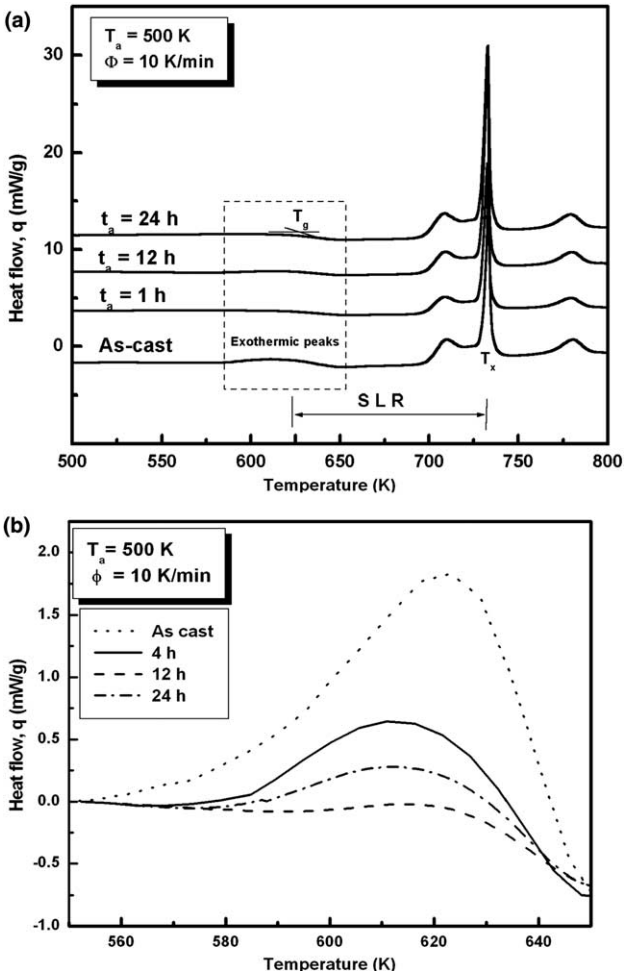

Fig. 2. (a) DSC thermograms of as-cast and isothermally annealed $Zr_{41.2}Ti_{13.8}Cu_{12.5}Ni_{10.0}Be_{22.5}$ (T_a = 500 K); (b) enlarged view of the glass transition regime (shown by the dotted box in (a).

sample that is annealed at 536 K ($0.85T_g$) for 24 h (Fig. 3). There is an excess endotherm that occurs at the end of glass transition, possibly due to the dissolution of clusters with the short range ordering (SRO) (formed during annealing which is a manifestation of structural relaxation [16]) when the BMG undergoes a glass to super cooled liquid transition upon heating. This observation indicates that the possibility of SRO during the process of sub-T_g annealing cannot be ruled out.

Although all the isothermal DSC scans appear similar, closer examination of the glass transition regime (indicated by the dotted box in Fig. 2(a) and shown magnified in Fig. 2(b)) reveals subtle but systematic changes at the glass transition. A sharp exothermic peak is seen for the as-cast glass, whose height reduces systematically with t_a. Van den Beukel and Sietsma [17,18] have analyzed the DSC thermograms of a Pd-based metallic glass and developed a model that describes the functional form of the DSC curves based on free volume theory [3,4] in which a similar exothermic peak is observed. According to their model, for every super cooled liquid there exists an equilibrium free-volume, v_{fe}, at a given temperature, which is given by the equation,

$$v_{fe} = A(T - T_0), \tag{1}$$

where T_0 is the ideal glass temperature and A is proportionality constant. In the as-cast alloy an excess amount of free volume, $v_f > v_{fe}$, is frozen-in due to the non-equilibrium processing conditions, which during continuous heating in a DSC experiment annihilates and approaches v_{fe}. The reduction in v_f, gives rise to heat release ΔH, when the glass sample is heated in a DSC. It was experimentally verified by Slipenyuk and Eckert [19] that,

$$\Delta H \propto \Delta v_f. \tag{2}$$

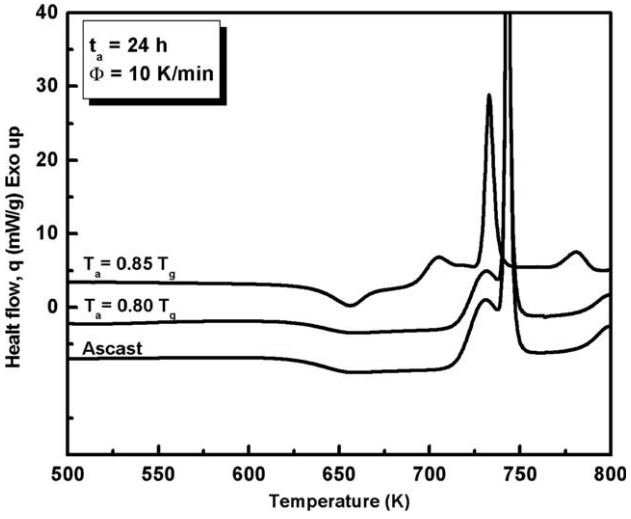

Fig. 3. DSC thermograms of the as-cast and isochronal annealed $Zr_{41.2}Ti_{13.8}Cu_{12.5}Ni_{10.0}Be_{22.5}$ (t_a = 24 h).

The exothermic peak seen before the glass transition in the as-cast alloy is the result of annihilation of excess free volume, Δv_f. Since the free volume gets reduced during the structural relaxation anneals, ΔH gradually decreases for the annealed samples. Hence, it is possible to estimate the free volume changes that occur during annealing by monitoring ΔH [17–19]. The ΔH associated with the exothermic peak was calculated by integrating the heat flow, q, (DSC thermogram) near the glass transition range (540–640 K). ΔH of each sample is normalized with the $\Delta H_{\text{as-cast}}$ of the as-cast alloy and is plotted as a function of the annealing time, t_a, and shown in Fig. 4(a). It is seen that $\Delta H/\Delta H_{\text{as-cast}}$ decreases by ~50% after annealing for 24 h.

The relaxation kinetics in metallic glasses are often found to obey the stretched exponential or Kohlraush–Williams–Watts (KWW) relaxation function [20] of the form,

$$\Delta H(t_a) = \Delta H_0 + (\Delta H_{\text{as-cast}} - \Delta H_0)\exp\lfloor -(t_a/\tau)^{\beta}\rfloor, \qquad (3)$$

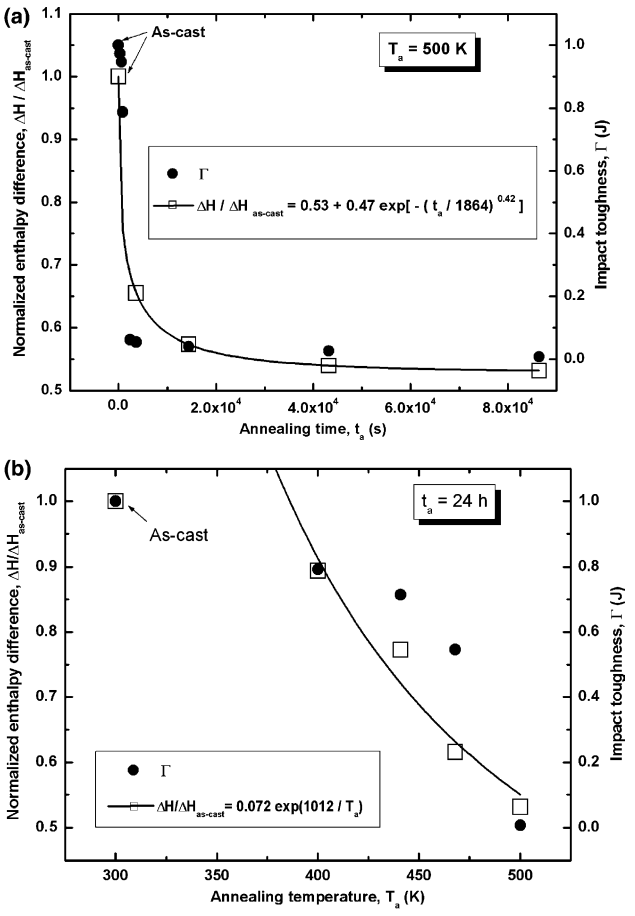

Fig. 4. Variation of the enthalpy difference, ΔH, and the impact toughness, Γ, (a) with the annealing time, T_a, in isothermal annealing (T_a = 500 K) and (b) with the annealing temperature, T_a, in isochronal annealing (t_a = 24 h).

where ΔH_0 is the enthalpy difference of the fully annealed sample, τ is the characteristic relaxation time, and β is the non-exponentiality parameter. A fit of Eq. (3) through the data with ΔH_0, τ and β as variable parameters yields $\Delta H_0 = 530$ J/g, $\tau = 1864$ s, and $\beta = 0.42$. The goodness of fit, R, is 1, indicating that Eq. (3) captures the isothermal relaxation behavior in BMGs accurately. The value of ΔH_0 is very close to that obtained after 24 h annealing, indicating that the relaxation is complete by that time. The β value extracted from the curve fit is similar to the value of 0.36 estimated by Suh and Dauskardt [14] in Vitreloy-1 at 573 K (0.36) and ~0.33 by Nagel et al. [21] in Vitreloy-4 ($Zr_{46.7}Ti_{8.3}Cu_{7.5}Ni_{10}Be_{27.5}$) samples annealed in the range of 450–500 K, both the measurements made using positron annihilation spectroscopy (PAS). Whereas $\beta = 1$ indicates that a single relaxation mechanism is operative, $\beta < 1$ implies that multiple relaxation mechanisms [20]. With respect to τ, Suh and Dauskardt [14] measure it to be $\tau \sim 25$ h whereas Nagel et al. [21] measure it to be ~30 min. Note also that a $\tau \sim 300$ s at $T_a = 500$ K for Vitreloy-1 was measured by Suh and Dauskardt [22] using DMA experiments. Clearly, the temperatures of annealing as well as the compositional differences play a significant role in determining τ.

Fig. 4(b) shows the variation of $\Delta H/\Delta H_{\text{as-cast}}$ with T_a for the isochronal annealing experiments with $t_a = 24$ h. As seen, the $\Delta H/\Delta H_{\text{as-cast}}$ gets reduced gradually with increasing T_a. The data are fitted with an Arrhenius function of the form,

$$\Delta H(T_a)/\Delta H_{\text{as-cast}} = A_0 \exp(E_f/RT_a), \qquad (4)$$

where A_0 is a constant and E_f is the activation energy. A curve fit through the data gives an $E_f \sim 0.085$ eV, which is similar to the 0.1 eV reported by Suh and Dauskardt [22] for temperatures below the T_g, obtained using a Arrhenius fit through the τ vs. testing temperature data collected using mechanical relaxation experiments. Since E_f is only ~3 times larger than k_BT (where k_B is the Boltzman constant) at room temperature, it indicates that very low thermal energies are enough for structural relaxation through free volume annihilation.

The rate of decrease of free volume during annealing is given by Tsao and Spaepen [23] as,

$$\frac{dc_f}{dt} = -kc_f(c_f - c_{fe}), \qquad (5)$$

where $c_f = \exp(-1/v_f)$, which is defined as defect concentration and k is a rate constant of the form,

$$k = C_0 \exp(-E_f/RT), \qquad (6)$$

where C_0 and E_f are variable parameters.

Recognizing that the free volume concentration is related to the viscosity of the glass, η, Spaepen [5] derived the following equation:

$$\eta \propto \exp(\gamma v^*/\bar{v}_f), \tag{7}$$

where v^* is the minimum free volume that must be available for an atomic jump, γ is a geometric factor and $\bar{v}_f$ is the mean free volume. Masuhr et al. [24] conducted the viscosity experiments on Vitreloy-1 and obtained the following values: $\gamma = 0.105$ and $\bar{v}_f/v^* = 0.1$ for the as-cast alloy. It is seen from Fig. 4(a) and (b) that there is a reduction of ~50% in the ΔH after annealing the samples at 500 K for 12 h. Assuming that $\Delta H \propto \bar{v}_f$, and substituting the values for γ and $\bar{v}_f/v^*$ from [24], in Eq. (7) suggests η must increase by ~300%. To ascertain this hypothesis, DMA has been performed to measure the changes in the internal friction, $\tan\delta$, on the as-cast and annealed ($T_a = 500$ K and $T_a = 4$ and 12 h). Assuming linear viscoelasticity, (i.e. the stress–strain relation is given by $\eta\dot{\varepsilon} + E\varepsilon = \sigma_0\cos(vt)$ where ε is the strain, σ_0 is the stress amplitude and v is the applied frequency, whose solution is $\varepsilon = \varepsilon_0\cos(vt + \delta)$), the relation between η and $\tan\delta$ is obtained as [25],

$$\eta = E/(v\tan\delta). \tag{8}$$

Fig. 5(b) shows the variation of η with the applied frequency, v (computed with $E = 96$ GPa). (This value was obtained from the instrumented indentation as well as DMA experiments in this work, which is also consistent with that reported in the literature [27].) It is observed that upon annealing at 500 K for 12 h, the room temperature η of the as-cast alloy increases only by ~30%.

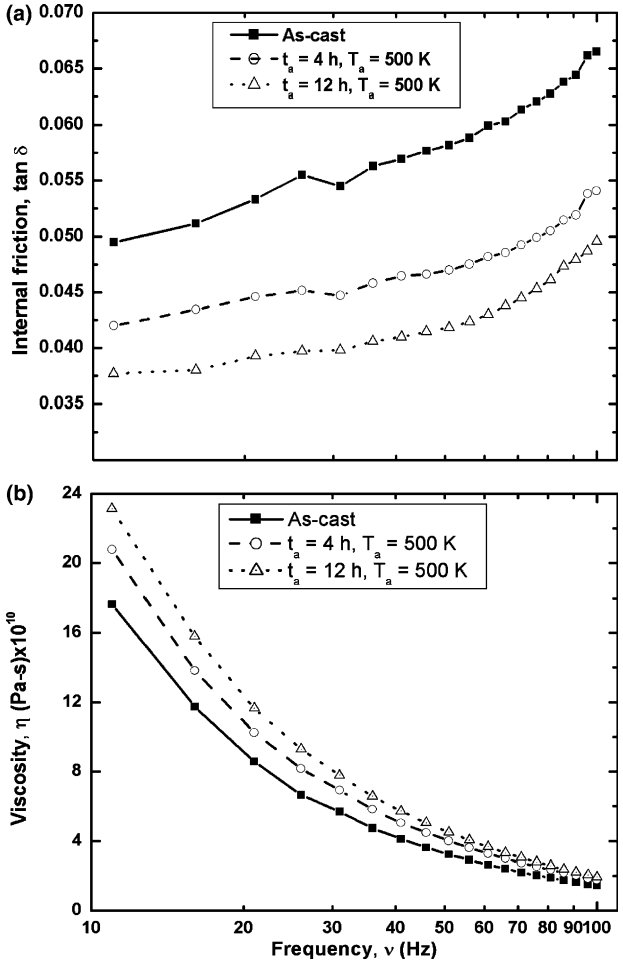

Fig. 5. Variation of the (a) internal friction, $\tan\delta$, and (b) viscosity, η, measured using the DMA for the isothermally annealed $Zr_{41.2}Ti_{13.8}Cu_{12.5}Ni_{10.0}Be_{22.5}$ ($T_a = 500$ K).

4. Embrittlement

Variations in the impact toughness, Γ, with t_a for isothermal annealing and with the T_a for isochronal annealing are shown in Fig. 4(a) and (b), respectively. These results show a severe embrittlement with annealing as reflected by a loss of Γ by nearly two orders of magnitude after annealing the specimens for 1 h at 500 K. There is a ~10% reduction in Γ even when the samples are annealed only at 403 K ($0.65T_g$) whereas the sample annealed at 536 K ($0.85T_g$) has a Γ that is below the machine specified limit (0.001 J). The observation that some loss in Γ is seen even at 403 K clearly demonstrates the limitation that structural relaxation induced embrittlement imposes on the service conditions of components made of BMGs.

As seen from Fig. 4(a) and (b), the variations in Γ with t_a and T_a are remarkably similar to that seen in $\Delta H/\Delta H_{as\text{-}cast}$ with t_a and T_a, respectively. This striking similarity between Γ and ΔH variations suggests that the loss of free volume during the structural relaxation is the reason for the embrittlement of BMGs.

As a complement to the impact tests, quasi-static toughness measurements were performed on the as-cast and the annealed alloys ($T_a = 500$ K, $t_a = 24$ h), with the aim of examining if the high loading rate of the impact tests is the cause of the observed severe embrittlement. Results presented in Table 1 indicate that the Γ of the annealed alloys ($T_a = 500$ K, $t_a = 24$ h) is ~90% lower than that measured for the as-cast alloy, clearly implying that the impact tests reflect intrinsic changes to the toughness.

Fracture morphologies of the as-cast and annealed samples ($T_a = 500$ K, $t_a = 24$ h) are markedly different as shown in Fig. 6. The fracture surface of the as-cast alloy (Fig. 6(a)) exhibits vein morphology that is typically

Table 1
Results of quasi-static 4-point bend tests on notched specimens

Material condition	Maximum bending stress (GPa)	Maximum bending strain (%)	Toughness, Γ (J)
As-cast	11.2	3.8	1.17
Annealed $T_a = 500$ K, $t_a = 24$ h	2.8	1.5	0.13

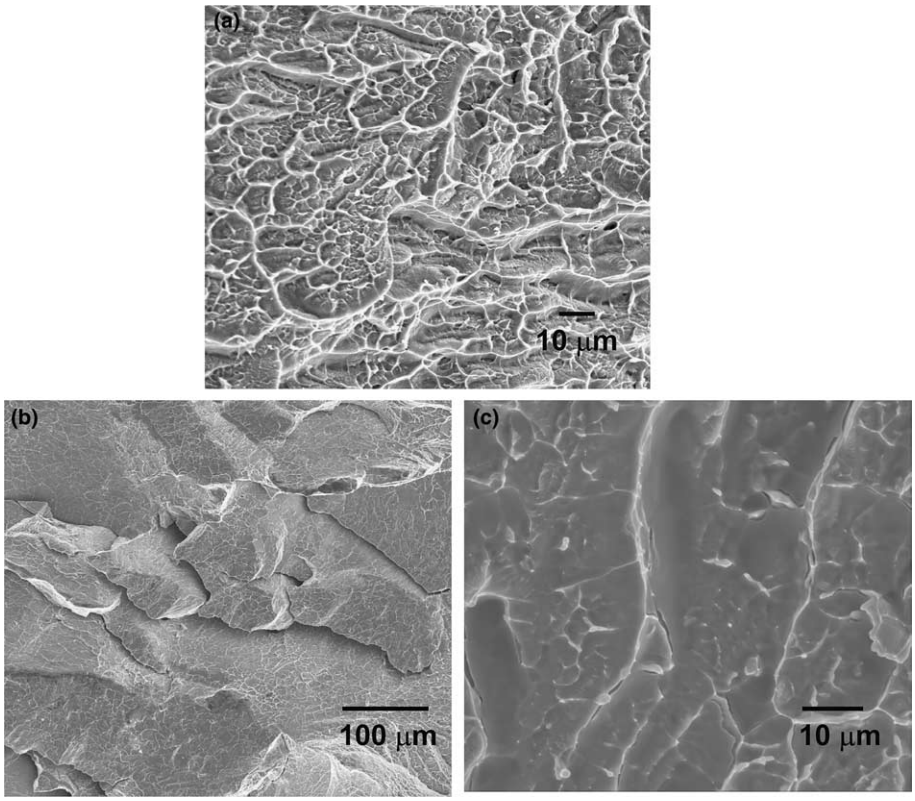

Fig. 6. SEM fractographs of the (a) as-cast and (b) annealed (T_a = 500 K, t_a = 24 h) alloys; (c) high magnification image of (b).

seen in the fractographs of metallic glasses. A gradual transition from these ductile fracture features to brittle features occurs with annealing. A low magnification image of the annealed alloy (T_a = 500 K, t_a = 24 h) shows that the cleavage fracture dominates. While the cleavage facets are also decorated with vein like features, they are considerably shallow (Fig. 6(c)) vis-à-vis that seen in the as-cast alloy. Examination of the side surfaces of the impact-tested specimens shows extensive shear banding at the root of the notch (Fig. 7). The annealed alloys are devoid of any such features, implying the lack of nonlinear deformation mechanisms for the mitigation of crack-tip stress concentration through shear banding in them.

Leamy et al. [26] proposed a deformation mechanism in which flow in metallic glasses occurs due to local adiabatic heating that leads to melting. But many subsequent researchers proved that the temperature increase during deformation is insufficient for localized melting to occur [27,28]. Gilbert et al. [29] observed that Vitreloy-1 sample fractured with emission of bright sparks upon impact testing in air whereas no sparks were seen when tested in nitrogen atmosphere. They argued that along with oxidation induced heat generation, intense heat was also generated due to plastic work. They concluded that heat emitted by the deformation was enough for local temperature to exceed 935 K, at which the metallic glass liquefies. Observations of highly localized deformation in the glass and surface re-melting provide support this argument. Further, we note that while sparks were also observed during the impact fracture of the as-cast samples, they were completely absent in

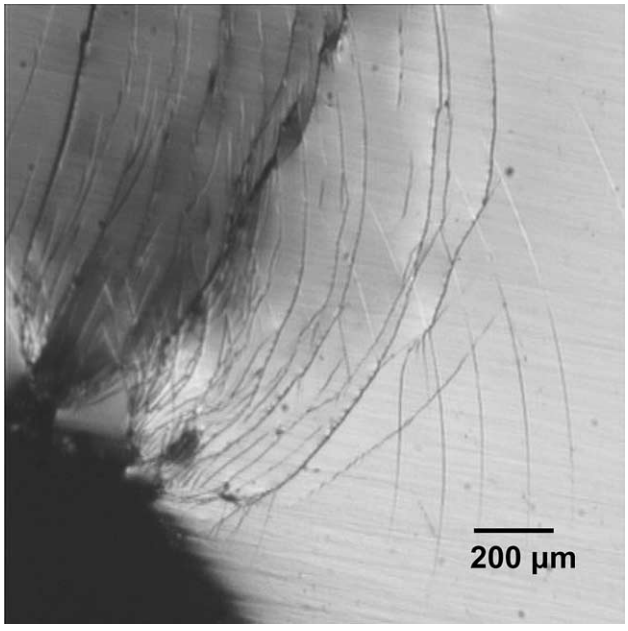

Fig. 7. An optical micrograph of the notch root of the as-cast impact test specimen showing extensive shear banding.

the annealed (t_a > 1 h) samples. This implies that severe plastic deformation can be absent in the latter case, which is possibly the reason for the lack of toughness.

5. Instrumented indentation

The calorimetric and impact toughness experiments, presented and discussed in the preceding two sections, establish a direct connection between the losses in toughness upon structural relaxation to the annihilation of free volume. However, the changes to the micromechanisms that are responsible for the embrittlement still need to be identified. To gain further insights into differences in the plastic flow processes of the as-cast and structurally relaxed alloys, we have employed the instrumented indentation technique. This is because the microscopic plastic instabilities in BMGs such as shear bands lead to fracture in uniaxial loading (particularly in tension) and hence discerning the subtle differences will be difficult. Because the deformation underneath an indenter is intrinsically stable, i.e., the contact area always increases (unless intervened by cracking in case of brittle materials being indented with sharp indenters) with increasing depth of penetration of the indenter, indentation allows for the examination of the response of a given material under multiaxial loading conditions. The alloy annealed at 500 K for 24 h was chosen for contrasting with the as-cast BMG, and hereafter the study is focused on these two cases only.

5.1. Vickers indentation

Several recent papers on nanoindentation of BMGs that utilize sharp indenters (Vickers or Berkovich) report that the load, P, vs. depth of penetration, h, curves are decorated with discrete displacement jumps [30–33]. These 'pop-ins', varying between 2 and 40 nm, are attributed to the nucleation and propagation of shear bands underneath the indenter. In order to examine if there are any quantitative differences in the pop-in displacements, $h_{pop\text{-}in}$, between the as-cast and annealed alloys, nano-Vickers indentation experiments were conducted. Fig. 8(a) shows that both the P–h curves are similar, decorated with several displacement jumps, although the hardness of the annealed alloy is ~4% higher. The magnified view of a part of the loading segment (inset of Fig. 8(a)) shows that the displacement jumps in the annealed alloy are relatively flat vis-à-vis those seen in the as-cast BMG. This can be due the nucleation of multiple shear bands in the latter, which makes the pop-in events more dispersed in nature, whereas single shear bands form at each instant in annealed samples, making the displacement jump more discrete. However, no quantitative differences in $h_{pop\text{-}in}$ vs. h plots of the as-cast and annealed alloys can be seen (Fig. 8(b)).

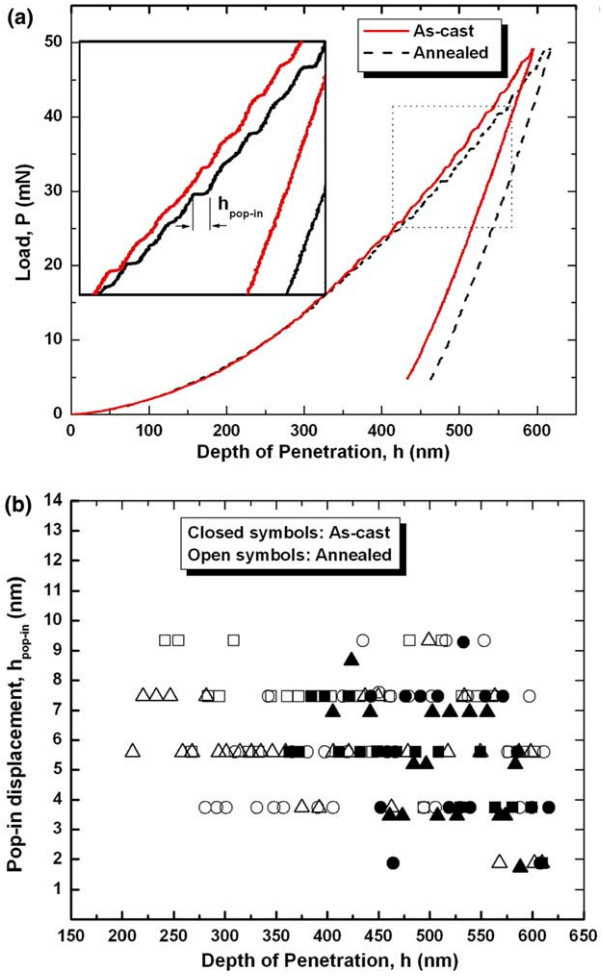

Fig. 8. (a) Nanoindentation response of the as-cast and annealed (T_a = 500 K, t_a = 24 h) $Zr_{41.2}Ti_{13.8}Cu_{12.5}Ni_{10.0}Be_{22.5}$ at a loading rate of 0.1 mN/s; (b) variation of the width of the pop-in displacements, $h_{pop\text{-}in}$, as a function of indentation depth, h.

Schuh et al. [30] report a linear increase in the $h_{pop\text{-}in}$ with increasing h in a Pd-based BMG and mentioned that they observed a similar trend in a Zr-based BMG. The linear increase was rationalized in terms of the strain rate dependence of the plastic flow coupled with the fact that increasing strain rate shows decrease in discrete pop-in events. Greer et al. [33] also report a similar trend in $h_{pop\text{-}in}$ vs. h and suggest that the scaling could be due to indentation strain rather than strain rate. They also speculated that the poor instrument resolution as a possible cause for the absence of pop-ins in the P–h curves recorded at high rates of loading. As seen from Fig. 8(b), the $h_{pop\text{-}in}$ is independent of h for the in Vitreloy-1, ranging between 2 and 9 nm with average values of 5.65 ± 1.74 and 5.50 ± 1.99 nm for the as-cast and annealed alloys, respectively. These values are similar to that seen at comparable h values in the data reported in literature. Note that the maximum depth of penetration, h_{max}, in our study is only ~600 nm whereas the

h_{max} levels reached by other researchers are much larger making it possible to fit a linear curve in their data.

Returning to the lack of quantitative differences in the $h_{pop\text{-}in}$ values recorded for the as-cast and annealed alloys, it is clear that the stress singularity at the tip of the Vickers indenter induces plastic deformation through shear banding even in the annealed material instead of cracking which is anticipated given the highly brittle nature of it. It is possible that the stress singularity at the indenter tip is mitigated through the homogeneous deformation of the glass, induced by the viscoplasticity that is generally dominant at low strain rates, followed by shear band nucleation. Since the measured η of the annealed sample is only ~30% higher than that of the as-cast sample, this scenario also appears more likely. This hypothesis is also supported by a close examination of the P–h curves (Fig. 8), which reveals that inhomogeneous deformation starts only at $h > 200$ nm. The high strains that prevail under the Vickers indenter (estimated to be equal to $\tan(19.7°) = 35.8\%$) thus promote shear banding.

To ascertain the role of homogenous viscous deformation further, in particular the strain rate dependence, instrumented micro Vickers indentation tests were performed at loading rates of 2 and 40 N/min. The P–h curves of the corresponding tests are shown in the Fig. 9(a) and (b). When the loading rate is high, both the as-cast and the annealed samples show almost identical P–h response (Fig. 9(b)) whereas the h_{max} is ~6.5% higher for the as-cast alloy as compared to that for the annealed alloy at 2 N/min (Fig. 9(a)). Surprisingly, the increase in hardness values of both the materials with the loading rate is similar, ~5.5% and 6% for the as-cast and the annealed alloys, respectively. This is due to the relatively higher nonlinear recovery during unloading of the as-cast alloy at 2 N/min (Fig. 9(a)). This possibly explains the small increase in hardness of the annealed sample. In summary, the Vickers microindentation test results confirm that the strain rate sensitivities of the two materials do not change significantly, with the as-cast BMG exhibiting a slightly higher sensitivity than the annealed BMG.

Optical microscopy of the indenter impressions led to some interesting observations, Fig. 10. In all the indents, irrespective of the material condition or the loading rate, the majority of the shear band activity is confined to one edge of the indent whereas there is at least one edge (typically the opposite one) that is completely devoid of any shear bands adjacent to it. Because of the deformation, the former edge appears curved (or "pin-cushioned") whereas the latter is straight. The other two connecting edges either show sporadic shear band activity or none at all. These types of features were common in many microindentation studies on different types of BMGs that others (see for example Fig. 8 of [33]) and we have conducted. Hence, it is unlikely that these features are

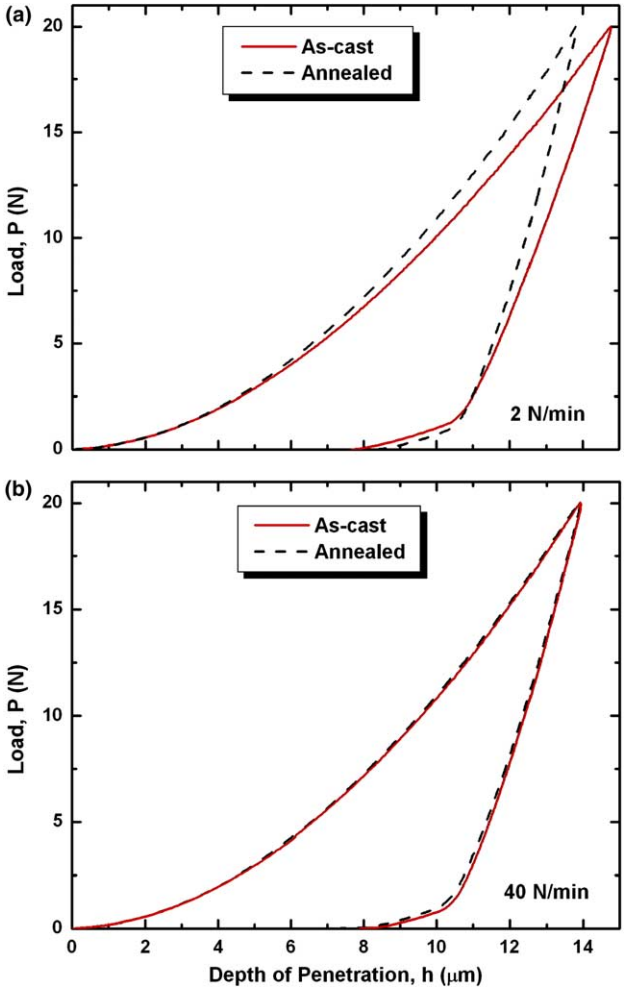

Fig. 9. Micro-Vickers indentation response of as-cast and annealed $Zr_{41.2}Ti_{13.8}Cu_{12.5}Ni_{10.0}Be_{22.5}$ at loading rates of: (a) 2 and (b) 40 N/min.

experimental artifacts (due to non-parallel face of the specimen that is being indented or misalignment of the indenter axis). It is believed that this asymmetry in deformation occurs as a result of the strain softening exhibited by metallic glasses. Several theoretical models show that shear band formation is associated with the creation of a net increase in the free volume, which coalesces into voids upon the removal of load [34,35]. Because of this, perturbation analysis show a precipitous drop in stress–strain curve once the shear bands initiate [36] and flow localizes in the vicinity of shear bands. Therefore, once shear bands initiate on one side of the Vickers indent, because of the strain softening on that, shear band activity tends to localize. In fact, nanohardness mapping of a prior deformed region underneath a spherical indenter in Vitreloy-1 by Bhowmick et al. [37] shows that the plastic region (with a high concentration of shear bands) is softer.

Qualitatively, the shear band density was found to be much larger in the as-cast alloy. In addition, the flow

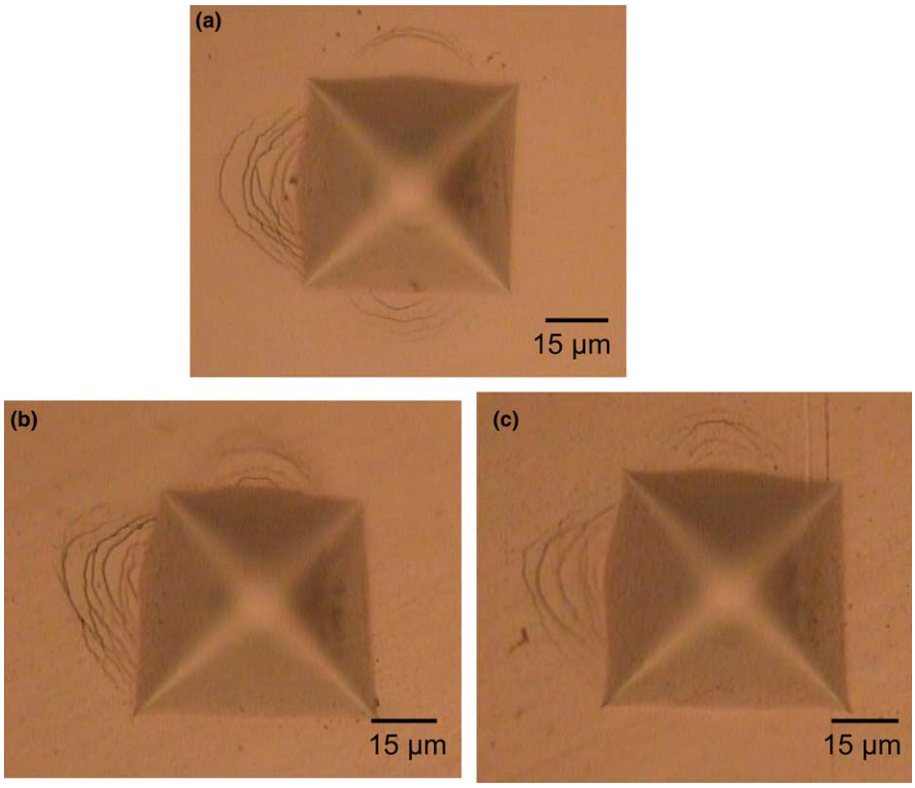

Fig. 10. Micrographs of the Vickers indents on: (a) as-cast, (b) annealed (2 N/min) and (c) annealed (40 N/min) $Zr_{41.2}Ti_{13.8}Cu_{12.5}Ni_{10.0}Be_{22.5}$.

lines in the annealed alloy found to be much smoother whereas their path appears to be tortuous in the as-cast alloy. This observation is consistent with the relatively horizontal pop-ins observed during nanoindentations of the annealed alloy. Morphologically, the shear banded regions in the as-cast alloy are similar for both the loading rates. However, the annealed alloy subjected to 40 N/min shows far lesser shear band activity vis-à-vis those which were tested at 2 N/min.

5.2. Spherical indentation

As mentioned earlier, the strain underneath the Vickers indenter is very large, inducing shear banding irrespective of the material condition. In contrast, spherical indentation offers the possibility of studying a given material's response as a function of indentation strain (estimated to be equal to the ratio of the half contact width, a, to the radius of the indenter, R). Therefore, instrumented spherical indentation was performed on both the as-cast and the annealed alloys to see if there are any differences in their response with the a/R. Because obtaining a well-defined spherical tip that is suitable for nanoindentation is difficult, we have resorted to microindentation studies.

The P–h curves obtained with various P_{max} are shown in Fig. 11. As seen, the P–h curves for the as-cast and annealed alloys are identical up to a load of 10 N.

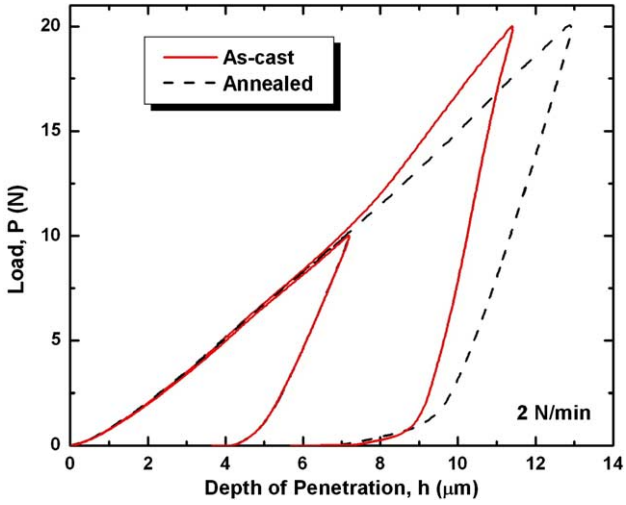

Fig. 11. Load, P, vs. depth of penetration, h, curves obtained using a spherical indenter in the as-cast and annealed $Zr_{41.2}Ti_{13.8}Cu_{12.5}Ni_{10.0}Be_{22.5}$.

When the load is increased beyond 10 N, hardening (i.e., increase in the slope of the loading curve) is observed in the as-cast alloy with a distinct 'knee' at a h of ~8 μm. (The reason for this hardening could be the extensive plastic flow through shear banding and hence pile-up of material around the indenter in the as-cast alloy. The increase in the contact area due to the pile-up

leads to an increase in the loading curvature and hence apparent hardening as more load is required to achieve the same contact pressure.) Variations of hardness, H, and normalized plastic depth (defined as the ratio of the total plastic depth of the indentation, h_p, to the maximum depth, h_{max}) with a/R are shown in Fig. 12(a) and (b), respectively. The Vickers indentation data are also plotted in these graphs. Again, the trends in both the as-cast and annealed alloys are similar, except for $a/R \sim 60\%$ ($P_{max} = 20$ N), where the as-cast alloy exhibits a ~20% increase in hardness vis-à-vis the annealed alloy.

Optical micrographs of the indents of both the as-cast and the annealed alloys taken after the indentation load of 10 and 20 N are shown in Figs. 13 and 14, respectively. At $P_{max} = 10$ N, the annealed alloy shows no shear band activity (Fig. 13(b)) whereas incipient shear bands are in the as-cast alloy (Fig. 13(a)), implying that the nucleation of shear bands in the as-cast alloys occurs more readily. Shear bands, whose shape resemble that of logarithmic spirals, appear at the edge of the indents of both the alloys. Careful counting of the shear bands

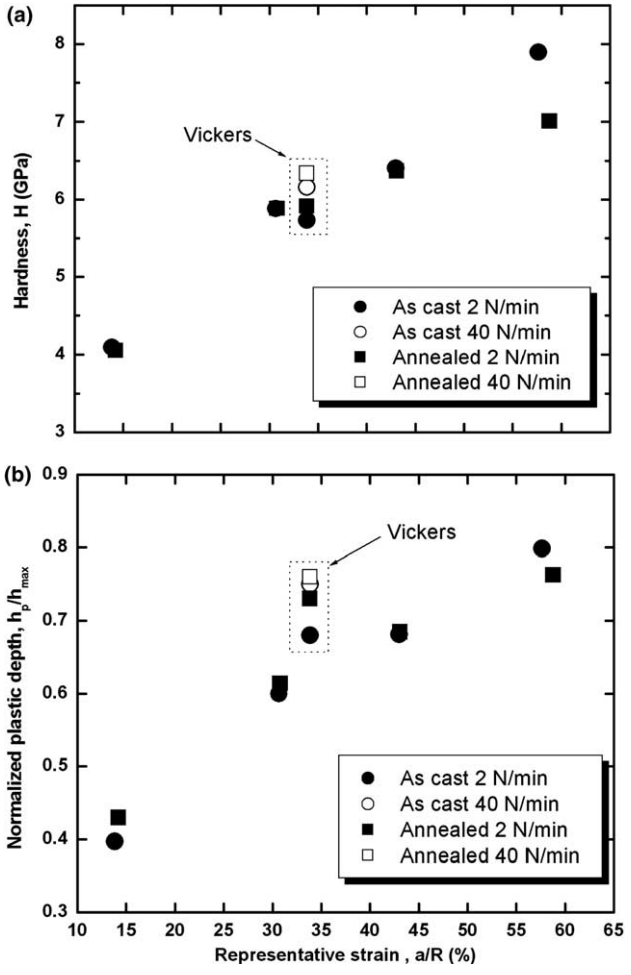

Fig. 12. (a) Hardness, H and (b) normalized plastic depth, h_p/h_{max}, plotted as a function of the representative indentation strain, a/R.

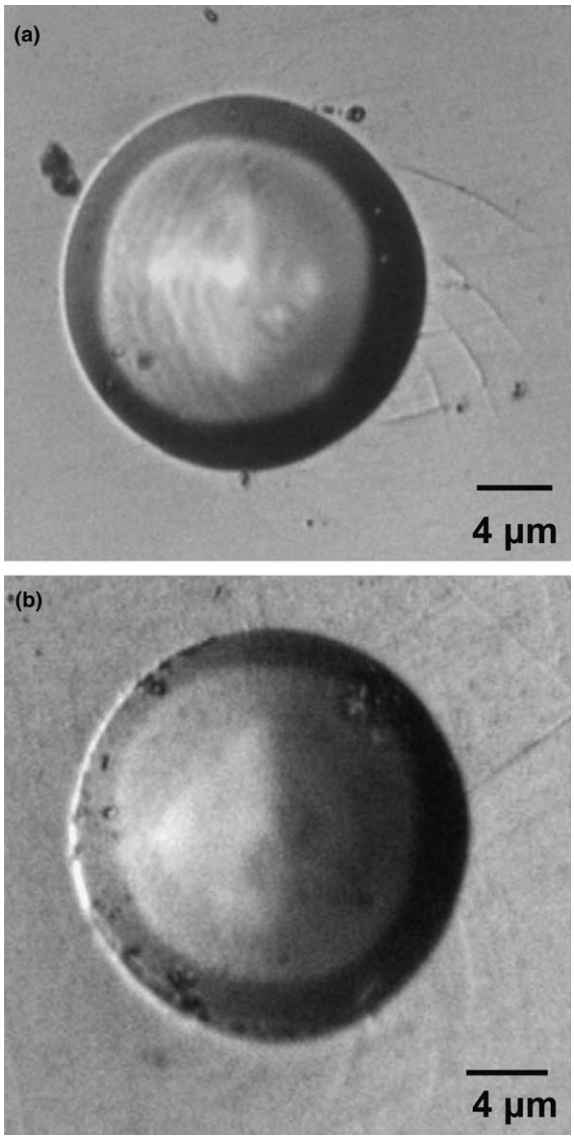

Fig. 13. Micrographs of the spherical indents on: (a) as-cast (b) annealed ($T_a = 500$ K, $t_a = 24$ h)$Zr_{41.2}Ti_{13.8}Cu_{12.5}Ni_{10.0}Be_{22.5}$ after applying a maximum load, $P_{max} = 10$ N.

indicates that their average number decreases from 30.8 ± 3.9 to 18.8 ± 2.7, i.e. by ~40%, upon annealing. Furthermore, a network of two families of slip lines can be seen, with an included angle of 79° in the as-cast alloy, which is representative of a material that obeys the Mohr–Coulomb yield criterion with a friction parameter of 0.19 [38].

The spherical indentation results clearly imply that while the plastic deformation at low strains in the as-cast and the annealed alloys is similar, it diverges at large strains. The fact that indenter impressions without much shear banding are seen in both the alloys for P_{max} of up to 10 N indicates that homogeneous plasticity of the material (through viscous flow) dominates at low strains. Since the measured viscosities of these two materials are similar, they respond similarly in this re-

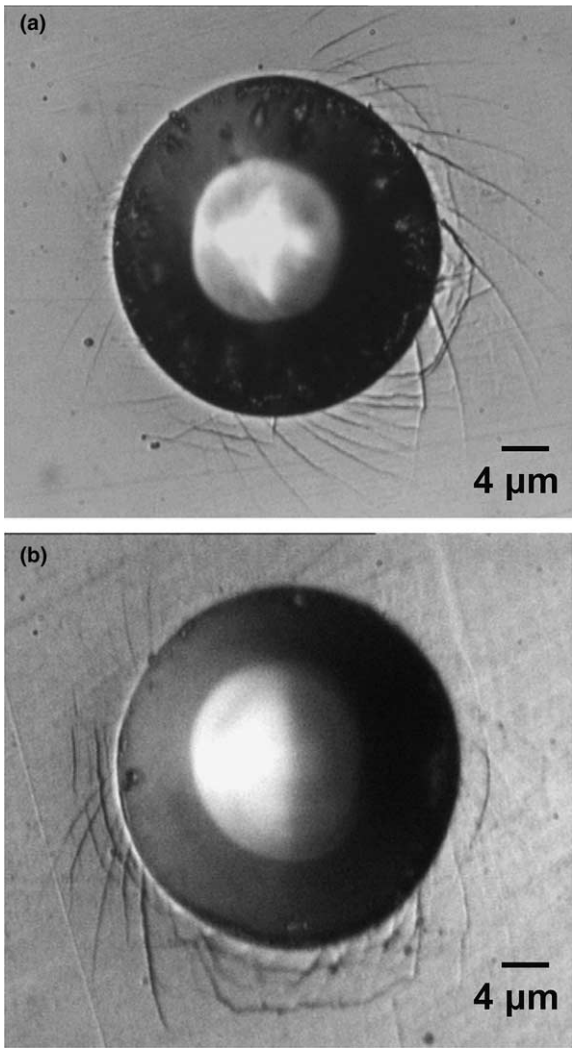

Fig. 14. Micrographs of the spherical indents on: (a) as-cast and (b) annealed ($T_a = 500$ K, $t_a = 24$ h)$Zr_{41.2}Ti_{13.8}Cu_{12.5}Ni_{10.0}Be_{22.5}$ after applying a maximum load, $P_{max} = 20$ N.

gime. However, at very large strains, the as-cast alloy can accommodate plastic deformation more readily through inhomogeneous flow since the propensity for shear band nucleation in this material is larger. Observation of a large number of shear bands at $P_{max} = 20$ N as well as the incipient shear bands around the indents of $P_{max} = 10$ N, support this argument. The larger amount of free volume that is available in the as-cast material favors this process. In analogy, the high stress concentration at the crack-tip of the as-cast alloy is mitigated by the relatively easy nucleation and propagation of many shear bands, leading to high toughness. The lack of such an extensive shear banding in the annealed alloy results in crack propagation with minimum energy consumption and hence the material fractures in a brittle manner.

Further, it is instructive to consider the differences between the types of loading in indentation and impact toughness and the attendant artifacts. While the indentation studies give information about a material's response primarily in compression, the material ahead of a notch tip in impact testing will experience tensile (or mode I) loading. Subtle differences in the plastic stress–strain response of the material can therefore get amplified, especially in the context of fracture. For example, the instability that sets-in due to the nucleation and propagation of a shear band leads to catastrophic fracture even in the as-cast material, resulting in negligible tensile ductility. Because of the stress concentration at the notch root, multiple shear bands nucleate and propagate simultaneously, imparting good toughness to the material. However, when the material is annealed, shear band nucleation is made difficult and hence the source of crack-tip plasticity gets severely limited, resulting in the loss of toughness.

Another aspect that is worth mentioning is that although embrittlement induced by sub-T_g relaxation appears to be common phenomenon in all the BMGs, some subtle differences exist. In a $La_{55}Al_{25}Cu_{10}Ni_5Co_5$ BMG, Ramamurty et al. [14] observe that Γ varies linearly with $\log(t_a)$ whereas in the present study (Vitreloy-1) an exponential decay in the toughness with t_a is noted. This is somewhat surprising since both are "metal–metal" type BMGs [39]. We speculate that the differences in relaxation induced embrittlement kinetics are possibly due to the presence of the Be atoms in Vitreloy-1, whose size is relatively small compared to the others in the alloy. Positron annihilation spectroscopy studies by Flores et al. [40] show that the free volume sites are associated with the Zr and Ti atoms in this alloy. Because of their small size, Be atoms can diffuse into these sites readily, thus enhancing the kinetics of free volume annihilation.

6. Summary

The susceptibility of a Zr-based BMG (Vitreloy-1) to embrittlement upon sub-T_g annealing was studied. A marked loss in impact toughness upon structural relaxation was seen, which corresponds well with the free volume changes that are characterized using DSC, implying that the free volume reduction is the fundamental cause for the embrittlement. However, DMA results imply that the changes of the viscosity, which depends on the free volume, are not as dramatic, suggesting that plastic flow through homogeneous deformation is similar in both the as-cast and annealed alloys. Results of various instrumented indentation tests show that the primary micromechanism responsible for the loss of toughness in the latter is the decreased propensity for shear band nucleation in them.

Acknowledgements

We are grateful to V. Shenoy, R. Narasimhan, S. Ranganathan, and R. Raghavan for many useful discussions. P. Padaikathan, S. Srinivasamurthy, A.N. Krishnamurthy, Gurulinga, S. Sasidara and S. Sashidara Pandit rendered skilful assistance in conducting the various experiments that are reported in this paper. We are thankful to N. Randall and R. Soden of CSM Instruments, Switzerland and B.S. Murthy of IIT-Madras, for their help with the instrumented indentation experiments. Financial support for this work was provided by a Grant from the Defense Research and Development Organization, Government of India.

References

[1] Klement W, Willens RH, Duwez P. Nature 1960;187:869.
[2] Chen HS. In: Luborsky FE, editor. Amorphous metallic alloys. London: Butterworth; 1983. p. 169.
[3] Wu T, Spaepen F. Phil Mag B 1990;61:739.
[4] Cohen MH, Turnbull D. J Chem Phys 1970;52:3038.
[5] Spaepen F. Acta Metall 1977;25:407.
[6] Spaepen F. J Non-cryst Solids 1978;31:207.
[7] Steif PS, Spaepen F, Hutchinson JW. Acta Metall 1982;30:447.
[8] Argon AS. Acta Metall 1979;27:47.
[9] Peker A, Johnson WL. Appl Phys Lett 1993;63:2342.
[10] Zhang T, Inoue A, Masumoto T. Mater Trans JIM 1991;32:1005.
[11] Telford M. Mater Today 2004(March):36.
[12] Suh D, Dauskardt RH. Ann Chim Sci Mater 2002;27:25.
[13] Suh D, Asoka-Kumar P, Dauskardt RH. Acta Mater 2002;50:537.
[14] Ramamurty U, Lee ML, Basu J, Li Y. Scripta Mater 2002;47:107.
[15] Wagner CNJ. In: Luborsky FE, editor. Amorphous metallic alloys. London: Butterworth; 1983. p. 169.
[16] Raghavan R, Basu J, Ranganathan S, Nishiyama N, Ramamurty U. Unpublished research.
[17] van den Beukel A, Seitsma J. Acta Metall Mater 1990;38:383.
[18] van den Beukel A, Radelaar S. Acta Metall 1983;31:419.
[19] Slipenyuk A, Eckert J. Scripta Mater 2004;39:44.
[20] Jackle J. Rep Prog Phys 1986;49:171.
[21] Nagel C, Ratzke K, Schmidtke E, Wolff J, Geyer U, Faupel F. Phys Rev B 1998;57:10224.
[22] Suh D, Dauskardt RH. J Mater Res 2002;17:1254.
[23] Tsao SS, Spaepen F. Acta Metall 1985;33:881.
[24] Masuhr A, Waniuk TA, Busch R, Johnson WL. Phys Rev Lett 1999;82:2290.
[25] Gittus J. Creep, viscoelasticity and creep fracture in solids. New York: Wiley; 1975.
[26] Leamy HJ, Chen HJ, Wang TT. Metall Trans 1972;3:699.
[27] Wright WJ, Saha R, Nix WD. Mater Trans JIM 2001;42:642.
[28] Wright WJ, Schwarz RB, Nix WD. Mater Sci Eng A 2001;319:229.
[29] Gilbert CJ, Ager JW, Schroeder V, Ritchie RO, Lloyd JP, Graham JR. Appl Phys Lett 1999;74:664.
[30] Schuh CA, Nieh TG. J Mater Res 2004;19:46.
[31] Schuh CA, Nieh TG, Kawumara Y. J Mater Res 2002;42:1651.
[32] Greer A, Castello A, Madge SV, Walker IT, Wilde JR. Mater Sci Eng A 2004;375:1182.
[33] Golovin YI, Ivolgin VI, Khonik VA, Kitagawa K, Tyurin AI. Scripta Mater 2001;45:947.
[34] Wright WJ, Hufnagel TC, Nix WD. J Appl Phys 2003;93:1432.
[35] Jing L, Spaepen F, Hufnagel TC. Phil Mag A 2002;82:2623.
[36] Huang R, Suo Z, Prevost JH, Nix WD. J Mech Phys Solids 2002;50:1011.
[37] Bhowmick R, Chattopadhyay K, Ramamurty U. Unpublished research.
[38] Patnaik MNM, Narasimhan R, Ramamurty U. Acta Mater 2004;52:3335.
[39] Basu J, Ranganathan S. Sadhana 2003;28:1.
[40] Flores KM, Suh D, Dauskardt RH, Asoka-Kumar P, Sterne PA, Howell RH. J Mater Res 2002;17:1154.